American Mineralogist, Volume 89, pages 1647–1654, 2004

Structure of the fluorapatite (100)-water interface by high-resolution X-ray reflectivity

CHANGYONG PARK,[1,*] PAUL FENTER,[1] ZHAN ZHANG,[1,2] LIKWAN CHENG,[1] AND NEIL C. STURCHIO[1,3]

[1]Environmental Research Division, Argonne National Laboratory, Argonne, Illinois 60439-4843, U.S.A.
[2]Department of Materials Science and Engineering, Northwestern University, Evanston, Illinois 60208, U.S.A.
[3]Department of Earth and Environmental Sciences, University of Illinois, Chicago, Illinois 60607, U.S.A.

ABSTRACT

A complete understanding of the surface chemistry of the apatite-water system requires direct observation of the interfacial structure at the molecular scale. We report results for the structure of the apatite (100)-water interface obtained with high-resolution specular X-ray reflectivity from a natural growth surface of Durango fluorapatite. A uniform termination at the crystallographic unit-cell boundary was determined. An atomistic model of the interfacial structure is compared to the experimental results and optimized through non-linear least-squares fitting in which the structural parameters were selected to be both physically and chemically plausible. The best-fit structure includes a Ca- and/or F-deficient outermost surface, minimal structural relaxations of the near-surface apatite crystal, and the presence of a layered interfacial water structure exhibiting two distinct water layers. The height of the first water layer is 2.64(9) Å relative to the relaxed surface with 3.5(1.3) water molecules per surface unit-cell area (64.9 Å^2). A second layer of adsorbed water is found 1.53(5) Å above the first layer, followed by a nearly featureless profile of the bulk liquid water. The layered structure of water is interpreted as being due to hydrogen bonding at the solid-water interface. The interfacial structure shows a strong similarity with the octacalcium phosphate structure projected along a surface normal direction.

INTRODUCTION

The structure and properties of the apatite-water interface have been widely studied as a basis for understanding the surface chemistry of apatite (Misra 1984; Posner 1985; Ishikawa 1997; Gramain and Schaad 2000; Dorozhkin 2002; Rakovan 2002). Apatite has received much attention in recent decades, as an analogue of bone and teeth of vertebrates, and as a major source of phosphorus for fertilizers. The apatite-water interfacial structure is also crucial for understanding various interfacial processes relevant to radionuclide waste management (e.g., Ordoñez-Regil et al. 1999; Teterin et al. 2000; Fuller et al. 2002) and heavy metal remediation (e.g., Jeanjean et al. 1995; Ma et al. 1995; Arey et al. 1999). The effect of hydration on surface structural relaxations and surface energy minimization has been discussed (Mkhonto and de Leeuw 2002). An interesting feature that arises among these studies is the idea that multi-layer adsorption of water is driven by hydrogen bonding at apatite surfaces (Posner 1985; Ishikawa et al. 1989). Yet, no direct molecular-scale observation of the structure of the apatite-water interface has been reported.

The structure of interfacial water for various mineral systems has been determined by surface X-ray reflectivity. Examples are water and calcite (Fenter et al. 2000a), barite (Fenter et al. 2001), alumina (Eng et al. 2001), muscovite (Cheng et al. 2001), quartz (Schlegel et al. 2002), and orthoclase (Fenter et al. 2000b, 2003). Most of these studies observed a single adsorbed water layer at the interface, typically due to completion of the substrate ion hydration shell. However, interfacial water with a distinct hydration layer followed by broader weak layering extending ~10 Å from the surface was observed for the muscovite-water interface (Cheng et al. 2001). In the present paper, we determine the interfacial structure of the fluorapatite (FAp) (100)-water interface with an emphasis on the hydration layer structure. The interfacial structure was obtained in the form of an electron density profile perpendicular to the FAp (100) surface, as derived from high-resolution X-ray reflectivity data. The validity of this approach has been established and used for various mineral-water interface systems (Fenter 2002). We found that the equilibrium structure of the FAp (100)-water interface in deionized water consists of (1) a Ca-and/or F-deficient outermost layer of the FAp whose surface is terminated at the traditional unit-cell boundary with minimal structural relaxations, and (2) two distinct adsorbed water layers, which are followed by a featureless profile corresponding to bulk fluid water. The hydration structure is discussed, and the role of the well-known metastable phase, octacalcium phosphate, in forming a stable hydration structure is re-evaluated.

FUNDAMENTALS

The X-ray reflectivity technique has been thoroughly described elsewhere (Als-Nielsen 1987; Feidenhans'l 1989; Fenter 2002), so only the essential elements are discussed here. The relationship between specular (mirror-likely reflecting) X-ray reflectivity and electron density can be expressed by the equation

$$R(Q) = \left(\frac{4\pi r_e}{QA_{uc}}\right)^2 \left|\int \rho(z)\exp(iQz)dz\right|^2 = \left(\frac{4\pi r_e}{QA_{uc}}\right)^2 \left|\sum_j f_j \exp\left(iQz_j\right)\exp\left[-\frac{1}{2}\left(Q\sigma_j\right)^2\right]\right|^2 = \left(\frac{4\pi r_e}{QA_{uc}}\right)^2 |F(Q)|^2 \quad (1)$$

* E-mail: cypark@anl.gov

where the wave vector $Q = (4\pi/\lambda)\sin(\alpha)$ is oriented along the surface-normal direction, and $\rho(z)$ is the corresponding electron density profile; α is the incident and outgoing angle with respect to the surface plane; λ is the X-ray wavelength.; $r_e = 2.818 \times 10^{-5}$ Å is the classical electron radius; and A_{uc} is the surface area of the unit cell. In the second expression, f_j, z_j, and σ_j are the atomic scattering factor, the position, and the vibrational amplitude of the jth atom, respectively; the integration is replaced with a summation over all contributing atoms in the unit cell. This expression can be rewritten as

$$R(Q) = \left(\frac{4\pi r_e}{QA_{uc}}\right)^2 \left|F_{bulk\text{-}uc}F_{CTR} + F_{interf} + F_{water}\right|^2 \quad (2)$$

where $F_{bulk\text{-}uc}$ represents the structure factor of a single bulk unit cell; F_{CTR} is the phase factor associated with the semi-infinite extension of the crystal, having the form of $F_{CTR} = 1/[1 - \exp(-Qd_{uc})]$, where d_{uc} represents the spacing of the lattice plane of the unit cell; F_{interf} includes contributions from all atoms whose positions may deviate from the ideal bulk lattice structure and from any adsorbed species at the mineral surface structure; and F_{water} is the semi-infinite sum over the atoms in the fluid water above the interfacial region. In parameterizing the structure factors, contributions from the semi-infinite solid substrate are described by the known bulk crystallographic parameters; thus, the unknown aspects of the structure correspond to the displacements of the interfacial atom locations, the occupation of each component (e.g., due to defect formation on solid surface), and the location and occupation of any adsorbed water layers near the solid surface. The derived structure is given in the form of an electron density profile.

The interfacial structure factor may be defined by the summation of all contributing atoms in the interfacial region as follows:

$$F_{interf}(Q) = \sum_j^{substrate} \theta_j f_j \exp\left[iQ(z_j + \Delta_j)\right]\exp\left[-\frac{1}{2}(Q\sigma_j)^2\right] + \sum_j^{adsorption} \theta_j f_j \exp\left(iQz_j\right)\exp\left[-\frac{1}{2}(Q\sigma_j)^2\right] \quad (3)$$

where θ_j is the atomic occupation factor at the position z_j and Δ_j is the relaxation of the atoms in the near-surface region. The interfacial region is defined as the region, both above and below the mineral surface, whose structure may differ from what is expected for the bulk crystal and the bulk water. Water species (e.g., H_2O, H_3O^+) adsorbed to the solid surface are included in the interfacial term (Eq. 3).

The fluid water structure is modeled to allow for any perturbations of the fluid water structure near the interface. The simplest model for the interfacial water profile corresponds to the featureless bulk water model described by an error function profile:

$$F_{water}(Q) = \rho_{water}A_{uc}\sum_j^{water} f_j \exp\left(iQz_j\right)\exp\left[-\frac{1}{2}\left(Q\sigma_j\right)^2\right]\frac{i}{Q} \quad (4)$$

where ρ_{water} is the average number density of water (0.033 Å^{-3}). This featureless water model contributes a simple $1/Q^2$ term to the reflectivity, where i/Q is the Fourier transform of an error function.

A more general model of the interfacial water structure consists of a semi-infinite stack of water layers with a fixed average density, constant layer spacing, d_{water}, but with a root-mean-square width that increases with the distance to the interface. The semi-infinite extension of these discrete layers produces the fluid water structure factor as shown by

$$F_{water}(Q) = \theta_{water}\sum_j^{water} f_j \exp(iQz_j)\exp\left[-\frac{1}{2}\left(Q\sigma_j\right)^2\right]\frac{1}{1-\exp(iQd_{water})\exp\left[-(Q\bar{\sigma})^2/2\right]} \quad (5)$$

where $\bar{\sigma}$ specifies how quickly the width of individual layer increases as the distance from the interface increases, and the atomic occupation factor for water, θ_{water}, per A_{uc} is adjusted to maintain the average bulk water density (i.e., $\theta_{water} = \rho_{water}A_{uc}d_{water}$). The electron density profile based on this description may produce water density profiles varying from an error-function-like profile to one with a sharp peak followed by rapid decay of oscillations. The range and strength of water "layering" are controlled primarily by $\bar{\sigma}$. This layered water model has the flexibility to represent water structure near the solid surface from a "featureless" to a "layered" structure with the same formulation. Unlike the error-function model, the structure factor for layered water exhibits a peak at $Q = 2\pi/d_{water}$ whose magnitude and width depend on $\bar{\sigma}$.

Except for f_j, the parameters included in the summations in Equations 3, 4, and 5 are taken as variables to fit experimental data. Parameters for extrinsic factors include an overall normalization constant c, a parameter that describes surface roughness (Robinson 1986) β due to crystallographic steps on the surface, and the thin-film water thickness t to describe the angle-dependent X-ray absorption by bulk water (Fenter 2002) $\mu(t,Q)$. The final form including all these parameters to model the experimental observation of specular X-ray reflectivity is obtained as follows:

$$R_{obs}(Q) = c\frac{(1-\beta)^2}{1+\beta^2-2\beta\cos(Qd_{uc})}\mu(t,Q)\left(\frac{4\pi r_e}{QA_{uc}}\right)^2\left|F_{bulk\text{-}uc}F_{CTR} + F_{interf} + F_{water}\right|^2 \quad (6)$$

Materials and experimental details

The material used in this study is gem-quality natural FAp from Cerro de Mercado, Durango, Mexico. The sample was taken from a rock specimen (courtesy of J.V. Smith, University of Chicago) containing individual crystals, ~2–3 mm wide and ~5–6 mm long in a rock matrix, which dominantly show the hexagonal prismatic (100) and hexagonal dipyramidal (101) faces. The crystal system of FAp is hexagonal, and the space group is $P6_3/m$ (see Young et al. 1969; Hughes et al. 1989; Elliot 1994 for mineralogical and crystallographic details). The chemical composition of the bulk crystal was analyzed as $Ca_{9.77}(P_{1.02}O_4)_6F_{2.08}Cl_{0.12}$ for major elements using EPMA (Geller MicroAnalytical Laboratory, JEOL Superprobe 733) taking the average value over randomly selected locations on a thin section perpendicular to **c**. A supplemental investigation for minor elements (courtesy of I. Steele, Electron Microprobe Laboratory, University of Chicago) reveals trace-substituent $(La_{0.03}Ce_{0.04}Sr_{0.007}Fe_{0.003}Si_{0.06})_{\Sigma 0.14}$ per unit cell. The atom locations and the anisotropic thermal vibrations data used in this paper were taken from Hughes et al. (1989). We measured the spacing of the (100) lattice plane as $d_{100} = 8.167$ Å, compared to the value of 8.135 Å from Hughes et al. (1989). A picture of the sample and a perspective view of an ideal FAp unit cell are shown in Figure 1. Apatite crystals do not show distinct cleavage, but the presence of optically flat natural growth surfaces suggested that atomically smooth surfaces might be available on these growth faces, similar to those observed in previous measurements of the quartz-water system (Schlegel et al. 2002). Figure 2 shows a typical image of the surface from which X-ray reflectivity was measured in this study, taken by contact-mode scanning probe microscopy (SPM) with a MultiMode™ SPM (Digital

Instruments). The orientation of the macroscopic steps is primarily along the **c** direction, and the step heights are as large as a few tens of nanometers. Numerous unit-cell-high steps are also observed. The lateral dimension of flat terraces typically exceeds a few micrometers, which indicates the suitability of this sample for X-ray reflectivity measurements. Qualitative examination comparing SPM images and X-ray reflectivity data for various FAp (100) specimens revealed that high-quality SPM images (as seen in Fig. 2) are a prerequisite for identifying a uniform FAp (100) surface to be probed by X-ray reflectivity. The use of X-ray reflectivity to study the termination of a crystal surface is described in the next section.

The crystal surfaces were cleaned ultrasonically with methanol and then deionized water, each for an hour, just after the sample was taken from the rock specimen. The cleaned samples were kept in air at room temperature, then exposed to deionized water for at least 12 h before they were mounted in a cell for the X-ray reflectivity measurements. In the cell, a thin film typically with a few tens of micrometers of deionized water forms on the solid surface just underneath an 8 μm thick Kapton™ film, which holds the sample. The influence of macroscopic steps, as seen in Figure 2, on the X-ray reflectivity data (e.g., due to shadowing of the surface) was minimized by aligning the beam direction along the steps, which are parallel to **c**. Other contributions to the X-ray reflectivity from the surface morphology, including microscopic step distributions and point defects, were evaluated through the Robinson roughness factor (Robinson 1986, see Eq. 6).

The X-ray reflectivity measurements were undertaken at an insertion-device station, beamline 11-ID-D (BESSRC-CAT) of the Advanced Photon Source at Argonne National Laboratory. The sample cell configuration and the specular geometry of the X-ray experiments are the same as those used previously (Fenter et al. 2001). A monochromatic X-ray beam with a wavelength of 0.827 Å (photon energy of 14.991 keV) was used. The photon energy was chosen with a sagitally focusing Si (220) monochromator, and a Pt-coated harmonic rejection mirror was used to vertically focus the beam. The incident beam flux was ~6×10^{10} photons per second after an aperture of 0.4 mm (vertical) by 1.2 mm (horizontal) placed before the sample. A smaller incident beam size (0.06 mm vertical) was used to avoid beam spill-off at small incidence angles (<5°). The reflected flux at each momentum transfer was measured using a scintillation detector, and the background-subtracted integrated intensity was determined at each scattering condition by measuring the rocking scan curves. The statistical uncertainty of the integrated intensities was calculated on the basis of the counting statistics of each data point in the rocking scan. A Gaussian function was used to fit the rocking-curve profiles. Only subtle differences were observed between the intensities derived from a Gaussian fit and a numerical integration, and no systematic differences were found. However, since reflectivity from natural growth surfaces may contain a number of potential sources of systematic error (e.g., inhomogeneous distributions of steps, the potential for a variation of surface composition, etc.), such errors can vary across the surface with the change of beam footprint during the reflectivity measurements. We therefore assumed that a minimum precision of the reflectivity measurement was not reflected in the counting statistics, and was estimated to be 7% of the reflectivity for each data point.

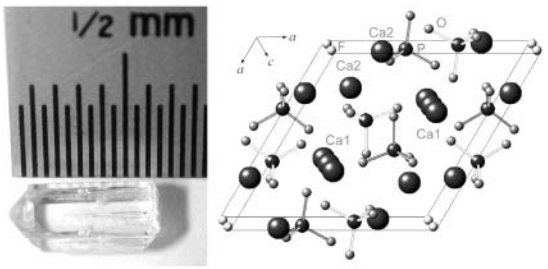

FIGURE 1. A picture of the natural fluorapatite crystal sample used in this study, showing the optically smooth growth faces, and perspective view of the hexagonal fluorapatite unit cell showing the (100) surface. Termination at the unit-cell boundary requires the exposed surface including extra O atoms to complete the phosphate tetrahedra.

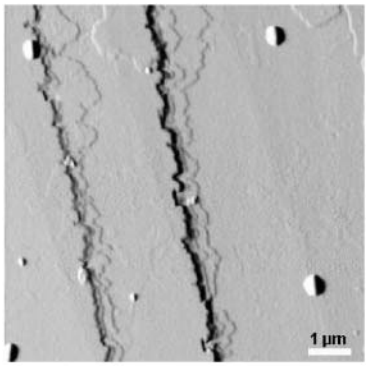

FIGURE 2. Contact-mode scanning probe microscopy images showing the typical distribution of steps and terraces of the (100) face investigated in this study.

RESULTS

Surface termination

As shown in Figure 1, the FAp unit-cell border intersects the PO_4 tetrahedra, with O atoms both above and below the boundary. The oxygen sites exposed by an arbitrary terminating plane to aqueous solutions are expected to undergo protonation reactions to form surface HPO_4^{2-} and/or $H_2PO_4^-$ ions (Berry 1967; Joris and Amberg 1971b; Ishikawa et al. 1989; Tanaka et al. 2000). Given the relatively complex crystal structure of FAp and the various possibilities for its terminating plane, we began our study by determining the surface termination. The first insight was obtained by comparing the data to model calculations near the FAp (100) Bragg peak. These data (solid squares in Fig. 3) show a characteristic dip at $Q \sim 0.8$ Å^{-1}, resulting from strong destructive interference just above the (100) Bragg peak. This

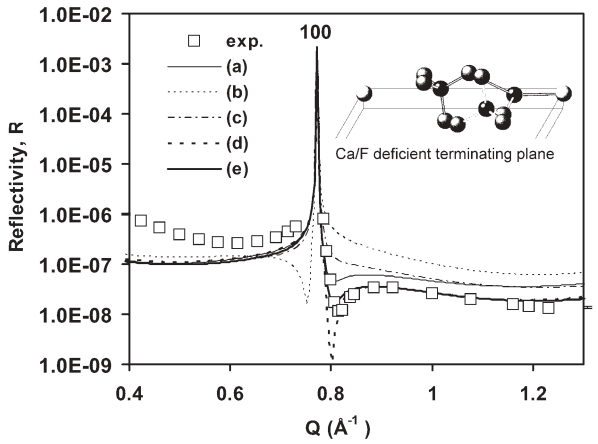

FIGURE 3. Comparison between the experimental and the calculated reflectivities near the (100) Bragg reflection for idealized FAp surface terminations: (**a**) a full unit cell terminated by calcium and phosphate ions; (**b**) a half unit cell terminated by phosphate ions; (**c**) a three-quarter unit cell terminated by calcium ions; (**d**) a full unit cell with partial depletion of surface phosphate ions; (**e**) a full unit cell with partial depletion of surface calcium and/or fluoride ions. Note that the position [either just above or just below the (100) reflection] and the depth of the intensity minima are sensitive to the different terminations. The experimental error bar sizes are all smaller than the symbol size.

type of interference, in particular, whether observed just above or just below the Bragg peak, has been previously identified as an indication of the surface termination of layered crystallographic lattices (Gidalevitz et al. 1997; Fenter 2000b; Ward 2001; Fenter and Park in preparation).

The reflectivities for various surface terminations in contact with featureless water were calculated for comparison to the experimental data (Fig. 3). In these calculations, the ion locations were given by their bulk crystallographic positions from Hughes et al. (1989), and comparisons were made to provide an initial indication of the correct terminating plane (e.g., half- or full-unit-cell termination) and of the deficiency of the surface. The atomistic configurations for the calculated surface terminations include: (1) a full unit cell terminated by calcium and phosphate ions, (2) a half unit cell terminated by phosphate ions, (3) a three-quarter unit cell terminated by calcium ions, (4) a full unit cell with partial depletion of surface phosphate ions, and (5) a full unit cell with partial depletion of surface calcium and/or fluoride ions, respectively. These results indicate that the natural growth surface of FAp is terminated at its full-unit-cell boundary. They also give an initial indication of the ion deficiency of the FAp surface. The calcium and fluoride ion depletion at the surface of the full-unit-cell termination (5) reproduces the characteristic dip very well. A simple representation of this termination is given in Figure 3 (inset). The only available information in the existing literature for the termination of FAp crystals is a molecular dynamics simulation that supports the three-quarter termination (3) as the most stable termination of the FAp (100) surface (Mkhonto and de Leeuw 2002). This result, however, is inconsistent with our X-ray reflectivity data, because it does not predict a dip above or below the (100) Bragg peak, whereas the data reveal a clear dip above the Bragg peak.

Each of the above calculations is based on an assumption that there is only one kind of termination on the surface. Thus, the appearance of such characteristic destructive interference in the experimental data and its consistency with calculated data indicates that the sample surface is terminated uniformly. The large discrepancy between experiments and calculations below the Bragg peak is because the calculations were done using an ideally terminated lattice. To get an initial indication of the uniformity as well as the location of the terminating plane, no parameter was varied to fit the experimental data except for the choice of the terminating plane, and the interfacial water structure was simply assumed as an error-function with arbitrary width and position. The full-unit-cell termination determined here provides guidance for configuring the initial parameters in the least-squares fitting. Our conclusions, therefore, must be considered to be indicative rather than definitive until they are tested against the complete reflectivity data set.

Models for FAp-water interface structure

The initial surface structure in the least-squares analysis was assumed to be a defective surface, in accordance with the above result, and it was represented by the depletion of one calcium ion and one fluoride ion at the FAp surface (Fig. 3). However, in optimizing the structural models, only the fractional occupation of the surface calcium ion was varied to represent the variations in the electron density at this lattice position. Because the X-ray reflectivity data do not provide element-specific structural information, and because the two contributions from calcium and fluoride ions were not resolved, the derived calcium occupation represents calcium and/or fluoride depletion or accumulation.

The water structure was modeled in three different ways: as featureless bulk water parameterized through Equation 4, as layered water described by Equation 5, and by a model with discrete adsorbed water molecules (the second summation item in Eq. 3) immediately followed by layered water. These three models were labeled as *featureless*, *layered*, and *discrete-layered*, respectively.

The model fits were performed with an error-weighted least-squares analysis. Comparisons between experimental results and the calculations are shown in Figure 4 for reflectivity R (top) and normalized reflectivity $R[Q\sin(Qd_{uc}/2)]^2$ (bottom). The latter was presented to emphasize the complex interference in the data for 3 Å^{-1} < Q < 4.5 Å^{-1}, indicated by arrows. The positions and patterns of the interference in the normalized reflectivity are indicative of structural modification and/or molecular adsorption on the solid surface. We found that the regions highlighted by the dashed ovals in Figure 4 are very sensitive to the adsorption of water molecules on the FAp (100) surface.

In presenting the optimized structural models, it is useful to plot the laterally averaged electron density profiles normal to the surface, as this is the quantity to which the specular X-ray reflectivity is directly sensitive. The corresponding electron density profiles, including both the outermost FAp layers and

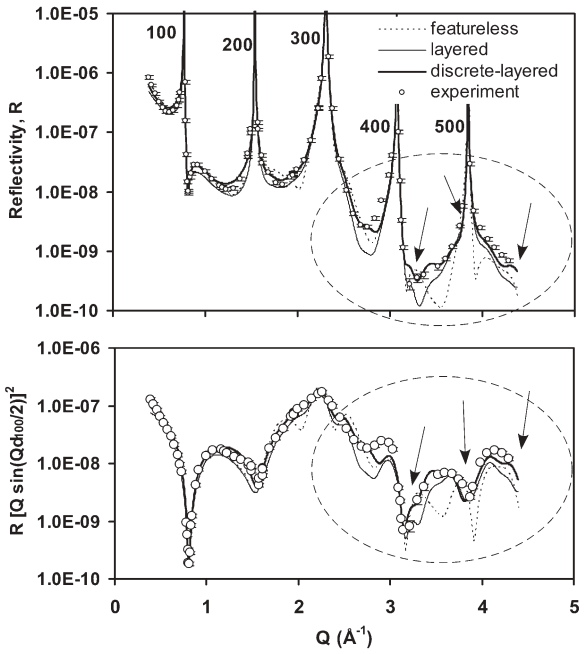

FIGURE 4. The experimental reflectivity data compared to the least-square model optimizations. The dashed ellipsoids highlight the high-Q region, which is especially sensitive to the different water adsorption models. The bottom panel shows normalized reflectivity to emphasize the complex interferences (indicated by arrows), which are obscured by the strong intensity variation due to the Bragg peaks (the top panel) but are highly sensitive to the interfacial water structure.

the interfacial water profiles, are shown in Figure 5. Here, the effective width of each atom's distribution was taken to be the intrinsic width, which is limited by the anisotropic thermal vibrational amplitude from Hughes et al. (1989), broadened in quadrature with a term representing the finite resolution of the experimental data (see Fenter et al. 2001; Fenter 2002).

The χ^2 values obtained from least-squares analysis were 27.1, 12.4, and 7.0 for the *featureless*, the *layered*, and the *discrete-layered* models, respectively. Comparison of these optimized structures to the experimental data is given in Figure 4. The first model, assuming the featureless bulk water profile (Eq. 4), fits the data very poorly, which indicates that the hydrated FAp (100) surface has a more complicated interfacial water structure than can be described by a simple error function profile, as is typical of most mineral-water interfacial systems (Fenter 2002). The layered water model in Equation 5 was introduced to provide some flexibility in representing the interfacial water structure. The thin solid line in Figure 4 represents the best-fit reflectivity for this model and shows better agreement with experimental results ($\chi^2 \sim 12.4$). In conformance with this model, structural relaxations of individual surface ions were allowed within the top surface layer, and below this, the unit-cell structure was allowed to uniformly expand or contract. Upon optimization based on this model, the water structure for the best-fit model has a tendency to produce a strong layering of water that decays slowly with distance from the FAp surface, which we find to be physically unreasonable. The final water model consists of two adsorbed water layers, followed by a layered structure for the bulk water. The optimization of this model provides the best fit to experimental data in this particular study ($\chi^2 = 7.0$). This model results in two discrete peaks in the water density profile near the FAp mineral surface, followed by a nearly featureless water profile at greater distances. Furthermore, this best-fit model shows only small structural relaxations near the FAp surface, especially in comparison to the previous models.

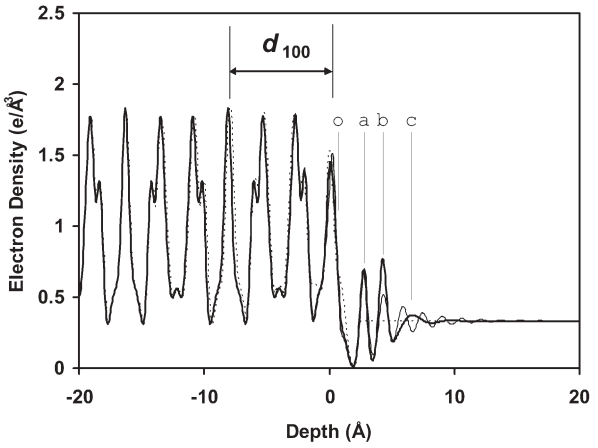

FIGURE 5. Electron density profiles obtained from the best-fit of each model (same legend in Fig. 4). The origin of the abscissa is located on the relaxed surface unit-cell boundary. The positional parameters for the best-fit discrete-layered model include the height of the first adsorbed layer at "a" 2.64(9) Å; the relative separation between the first and second adsorbed water layer $d_{a\text{-}b} = 1.53(5)$ Å; the relative separation between the second adsorbed water layer and the first layer of the bulk water $d_{b\text{-}c} = 2.03(1.41)$ Å; the average height of the outermost O atoms of the surface phosphates at "o", 0.54(15) Å.

The value of the optimized quality of fit ($\chi^2 = 7.0$) requires further analysis, because χ^2 values for error-weighted least-squares fitting are expected to converge to unity when the best fit result is obtained, although values of 2–5 are not uncommon (e.g., Fenter 2000b). Other possible combinations of adsorbed and bulk water structure (e.g., one adsorbed layer plus layered water or two adsorbed layers plus featureless water) were tested, but they showed only trivial differences from the final model presented here. No additional improvements in the quality of fit could be achieved without drastically changing the chemical composition and the lattice constant of the bulk FAp crystal, both of which were independently determined. Further optimization by distortion of individual surface phosphate ions in the near-surface region (i.e., bond lengths and angles and orientation) provided only limited improvement of the quality of fit, while at the same time the total number of parameters increased quickly and the estimated errors were strongly affected by co-variance of these parameters. We have obtained comparable data, within quoted errors, from separately measured FAp (100) samples analyzed with the same parameterization described above. Consequently, we expect the derived results to be intrinsic to the FAp (100)-water interfacial structure. The detailed results are described in the following sections.

Ca- and/or F-deficient surface

Acceptance of the initial FAp interfacial configuration, assuming the calcium- and fluorine-depleted surface has the full-unit-cell termination (Fig. 3), defines a partially depleted surface unit cell, $Ca_9(PO_4)_6F$, which does not satisfy the charge balance on its own. When the occupation factor for the remaining surface calcium ions is allowed to vary, the best-fit result gives the total number of calcium ions exposed at the surface as $\theta_{Ca} = 1.67(33)$ with fixed $\theta_F = 1.0$ (as compared to $\theta_{Ca} = 2$ and $\theta_F = 2$ per surface unit cell). Thus, the data are consistent with the model that describes partial depletion of calcium and fluoride ions at the surface. Since the surface calcium and the fluoride ions are not distinguished in this measurement, these two contributions are constrained by $Z_{Ca}\theta_{Ca} + Z_F\theta_F = 42.4$, where Z_i is the atomic number for element i. The smaller atomic number of fluorine compared to calcium (9 vs. 20) implies that certain amounts of calcium and fluorine (or a fluoride-substituting anion, e.g., OH^-) must be present in the outermost surface layer, ranging in coverage from 2.0 calcium and 0.27 fluorine atoms to 1.22 calcium and 2 fluorine atoms. Therefore, complete depletion of either calcium or fluoride ions from the outermost layer is not expected on the basis of these results. We expect, however, that cationic defects are accompanied by the absence of negative ions in order to maintain charge balance in the stoichiometric unit cell. Otherwise, it is possible to consider that the missing calcium ions may have been replaced by H_3O^+ ions, which demands minimal depletion of negative ions.

The calcium- and fluorine-depleted surface unit cell inferred in this study agrees well with the results of Brown and Martin (1999), which reported non-stoichiometric surface layer formation during hydroxyapatite (HAp) dissolution. According to

these authors, at steady state, HAp dissolves congruently only when the solution and solid have the same Ca/P ratio. A surface layer having a Ca/P ratio less than 1.67, which is often used as the indication of congruent dissolution of apatite, will form as a result of equilibration of stoichiometric HAp with water. The deficiencies on the FAp surface in this study result in a Ca/P ratio ranging from 1.54 to 1.67 for the outermost FAp unit cell, which agrees well with the above argument and with Ca/P values of ~1.50–1.67 for calcium-deficient apatites (Berry 1967; Joris and Amberg 1971a; Brown and Martin 1999). In this study, however, the deficiency was limited to the outermost atomic layer within ~2–3 Å of the FAp (100) surface.

Surface relaxation

While the occupation factors were varied only for the surface calcium ions, positions were varied for all surface atoms. The positions of all atoms in the top three unit cells were varied only by uniform expansion/contraction of the unit-cell dimensions. The net surface displacement was found to be less than +0.10(6) Å (i.e., outward from the surface, with 0.03, 0.03, and 0.035 Å relaxation for each layer, respectively, from the topmost unit cell). Therefore, deformation of the hexad channel, which is parallel to the surface, is minimized with less than ~0.03 Å displacement per unit cell along the surface-normal direction. We found that the top surface phosphate ions are displaced toward the bulk crystal [$\Delta_{PO4,\ avg}$ = –0.34(12) Å, where $\Delta_{PO4,\ avg}$ represents the average displacement of two differently oriented phosphate ions], while calcium coincides with the bulk-terminated lattice site within error [Δ_{Ca} = 0.01(14) Å], and the F ions are outwardly relaxed [Δ_{F} = +0.38(37) Å], relative to the relaxed top unit-cell boundary. The corresponding electron density profile of the best-fit structure (thick solid line in Fig. 5) does not show a significant difference with respect to the ideally terminated FAp lattice, except for the smaller peak height of the outermost FAp layer (at depth = 0 Å) mainly due to the depletion of surface ions. The peak position in the electron density profile for the surface ions almost coincides with that for the uniformly relaxed surface unit cell. Further studies that are sensitive to the lateral structure through non-specular reflectivity are required for a full description of the detailed surface modification.

Water adsorption

The two discrete water layers seen in Figure 5 are both essential features for reproducing the interference patterns in the highlighted Q region in Figure 4. These two discrete layers of water were described in the structure factors by two separate molecular layers that are followed immediately by layered bulk water. The height relative to the relaxed surface of the first adsorbed water layer is 2.64(9) Å (indicated by "a" in Fig. 5), and the second adsorbed layer is higher than the first (the distance between "a" and "b") by 1.53(5) Å. The derived number of water molecules is 3.5(1.3) and 4.1(2.2) per unit-cell area (A_{uc} = 64.9 Å^2) for the first and the second adsorbed layers, respectively. The parameters describing the root-mean-square width of the two adsorbed water layers [0.12(61) Å and 0.19(37) Å for the first and the second layer, respectively] show sharp discreteness, but with large estimated errors. When expressed in the form of an electron density profile (Fig. 5), the actual sharpness of the discrete layers is folded with the experimental resolution limit determined by the Q-range of the data ($2\pi/Q_{max}$ ~1.4 Å). The bulk water shows an almost featureless profile whose first layer is found 2.03(1.40) Å above the second adsorbed layer (the distance between "b" and "c"). The average spacing of the layered water was determined to be 2.38(4.81) Å, the large error indicating the lack of significant layering in the bulk water region, which is described by $\bar{\sigma}$ = 0.96(1.67) Å.

We explored the uniqueness of these models through different parameterizations. As mentioned above, the best-fit *discrete-layered* model can be derived from other combinations of adsorbed species and fluid water, but it still retains its essential feature of two layers of adsorbed water. These other models showed only minimal differences. For example, two adsorbed monolayers plus featureless bulk water model fit the data with χ^2 = 7.6, with comparable values for the positional parameters and errors quoted above.

Discussion

Hydrogen bonding and hydration structure

Surface protonation to provide surface P-OH functional groups (Berry 1967; Joris and Amberg 1971b; Ishikawa et al. 1989; Wu et al. 1991; Tanaka et al. 2000) is intimately related to hydrogen bonding. The discrete layering of water inherent in the *discrete-layered* model, therefore, is considered to be closely related to hydrogen bonding between O atoms of surface phosphate ions and the adsorbed water molecules (Posner 1985; Ishikawa et al. 1989). Posner (1985) pointed out that the number and orientation of the surface polar (P-OH) groups will determine the adsorption strength on apatite surfaces and will be directly related to those of water molecules available through hydrogen bonding. On the basis of their FTIR spectroscopy study, Ishikawa et al. (1989) reported that ~2 P-OH groups among the total ~2.9 P-OH groups per $A_{uc,\ HAp}$ interact with 3.3 water molecules (although it is not known if all these water molecules interact through hydrogen bonding). The number of water molecules that we derived here in the first adsorbed layer [3.5(1.3)] agrees well with this value. On the other hand, the inter-O atom distance between the first adsorbed layer and the average O atom layer of the surface phosphates was estimated to be 2.1(2) Å (the distance between "o" and "a" in Fig. 5), less than the mean van der Waals diameter of water (2.82 Å, Franks 2000) and far less than an intermediate peak radial distribution data value (~3.2 Å, Narten et al. 1967), which suggests a certain orientational configuration of the first layer water molecules.

Posner (1985) suggested that the influence of highly polar surface phosphate ions is the main cause of multi-layer water adsorption. This suggestion is based on observations of methanol adsorption on apatite, where the non-polar molecules do not show multi-layer adsorption. In this context, we may explain the multiple-discrete layers of adsorbed water as due to the effect of the polarity of surface phosphate ions into the water structure. A recent molecular dynamics and Monte Carlo simulation study of the water-MgO interface (McCarthy et al. 1996) showed that the probability distribution of the angular orientation of water molecules is strongly correlated with the layering of interfacial water at solid surfaces. Another MC simulation study of the water

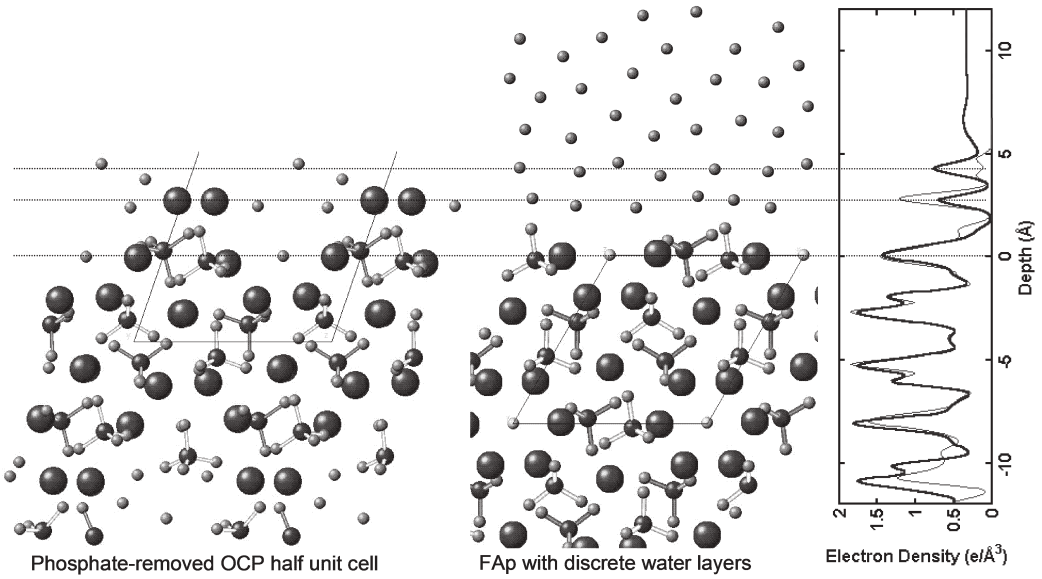

FIGURE 6. Illustration of the octacalcium phosphate (OCP) template on the FAp (100)-water interface. The half-unit-cell OCP with removed phosphate matches the hydration structure of the FAp (100) surface, replacing the structural calcium in OCP with water molecules. The water molecules are represented by O atoms; the thin line in the electron density profiles represents the OCP templates; the thick line represents the FAp hydration structure obtained in this study.

structure on the mica surface (Park and Sposito 2002) revealed that the water molecules contained in the layered hydration structure (Cheng et al. 2001) retains "persistent liquidity" but with strong lateral ordering. However, strong orientation effects related to weak hydrogen bonding on hydrophobic surfaces in liquid phases (Scatena et al. 2001) have recently been revealed. Thus, the effect of surface polarity into adjacent water is thought to be constrained with such orientational distributions.

In their experimental study of the water-mica interface, Cheng et al. (2001) interpreted the layered structure of hydration water to be due to the geometric confinement of the surface as "hard-wall". The local electrostatic field due to a fixed charge in the crystal lattice may also influence this atomic configuration. In the present study, the distance between the two adsorbed water layers (the distance between "a" and "b" in Fig. 5) was estimated to be 1.53(5) Å, substantially less than even the intermolecular distance for hydrogen bonding in liquid water (1.88 Å at 4 °C, Modig et al. 2003). If we think of the interfacial water structure in terms of close packing of hard spheres (representing water molecules) as well as the orientational configuration, a smaller interlayer spacing can be thought of as arising from the penetration of adjacent water molecules into the loosely packed water layer. The water layers starting from layer "b" in Figure 5, as for those in mica (Cheng et al. 2001), may be considered to be water in the bulk hydration layer. At a fundamental level, the distinction between the second adsorbed water layer and bulk water is ambiguous since their local electron densities are indistinguishable (~0.34 $e^-/Å^3$ vs. 0.33 $e^-/Å^3$, respectively), but distinct from that of the first adsorbed water layer (~0.28 $e^-/Å^3$). This suggests that the first water layer is a separate single layer and the hydration structure is connected to it through hydrogen bonding with a *generic* hard-wall effect. Note that hydrogen bonding plays a vital role in forming all of these structures.

Hydrous defective apatite structure

The revelation that octacalcium phosphate (OCP), $Ca_8H_2(PO_4)_6{\cdot}5H_2O$, the so-called "hydrous defective apatite", has its own crystalline form (triclinic, space group $P1$ or $P\bar{1}$, Brown et al. 1962) has led to continuing arguments concerning the role of OCP as a metastable precursor phase in the formation of thermodynamically stable HAp (e.g., Brown et al. 1981; Misra 1984; Liu and Nancollas 1997). The notion of a metastable template also seems to explain the observed formation of the water layers (Fig. 5) at the natural growth surface of FAp. The projection along the **c** of OCP, as seen in Figure 6, illustrates how this metastable mineral can be thought of as a precursor of apatite (see also Brown et al. 1981). Except for the replacement of F^- (or OH^-) ions with phosphate O atoms, the structure projected from the apatite crystal is found in the OCP structure (the dashed overlapping parallelogram). The replacement of calcium in the OCP half unit cell with water and the removal of some phosphate ions reproduce a structure very similar to the layered water structure derived for the FAp (100) surface. The local electron density profiles for the two structures are almost identical. The positions of water layers at the FAp surface correspond to the positions of structural water within OCP. Although the bonding characteristics and the charge properties between the two phases would likely be different, this comparison suggests that the layered structure of water on this particular surface can also be explained simply by its tendency to follow the OCP template, that is, to distribute the water molecules at the extension of an OCP-like structure having the "hydrous defective" form. Fundamental questions concerning how a defective structure forms a stable surface with minimal relaxations and why the first adsorbed layer is placed at that particular distance [2.64(9) Å] can be addressed by this surprising similarity.

ACKNOWLEDGMENTS

The X-ray reflectivity measurements were performed at beamline 11-ID-D at the Advanced Photon Source at Argonne National Laboratory (with additional preliminary measurements performed at beamline 12-BM and 1-BM). We thank J.V. Smith (University of Chicago) for graciously providing the rock specimen from which the apatite crystals were extracted, and I. Steele (University of Chicago) for graciously providing the electron microprobe analysis. Use of the Advanced Photon Source was supported by Office of Basic Energy Sciences under contract W-31-109-Eng-38. This work was supported by the Geosciences Research Program, Office of Basic Energy Sciences, U.S. Department of Energy.

REFERENCES CITED

Als-Nielsen, J. (1987) Solid and liquid surfaces studied by synchrotron X-ray diffraction. In W. Schommers and P. Von Blanckenhagen, Eds., Topics in Current Physics: Structure and Dynamics of Surfaces II, Vol. 43, 181–222. Springer-Verlag, New York.

Arey, J.S., Seaman, J.C., and Bertsch, P.M. (1999) Immobilization of uranium in contaminated sediments by hydroxyapatite addition. Environmental Science and Technology, 33, 337–342.

Berry, E.E. (1967) The structure and composition of some calcium-deficient apatites. Journal of Inorganic and Nuclear Chemistry, 29, 317–327.

Brown, P.W. and Martin, R.I. (1999) An analysis of hydroxyapatite surface layer formation. Journal of Physical Chemistry B, 103, 1671–1675.

Brown, W.E., Smith, J.P., Lehr J.R., and Frazier, A.W. (1962) Octacalcium phosphate and hydroxyapatite. Nature, 196, 1048–1055.

Brown, W.E., Mathew, M., and Tung, M.S. (1981) Crystal chemistry of octacalcium phosphate. Progress in Crystal Growth and Characterization of Materials, 4, 59–87.

Cheng, L., Fenter, P., Nagy, K.L., Schlegel, M.L., and Sturchio, N.C. (2001) Molecular-scale density oscillations in water adjacent to a mica surface. Physical Review Letters, 87, 156103(1–4).

Dorozhkin, S.V. (2002) A review on the dissolution models of calcium apatites. Progress in Crystal Growth and Characterization of Materials, 44, 45–61.

Elliot, J.C. (1994) Structure and Chemistry of the Apatites and Other Calcium Orthophosphates. Chapter 2, 63–110p. Elsevier, Amsterdam.

Eng, P.J., Trainor, T.P., Brown Jr., G.E., Waychunas, G.A., Newville, M., Sutton, S.R., and Rivers, M.L. (2001) Structure of the hydrated α-Al_2O_3 (0001) surface. Science, 288, 1029–1033.

Feidenhans'l, R. (1989) Surface structure determination by X-ray diffraction. Surface Science Reports, 10, 105–188.

Fenter, P. (2002) X-ray reflectivity as a probe of mineral-fluid interfaces: A user guide. In P. Fenter, M.L. Rivers, N.C. Sturchio, and S.R. Sutton, Eds., Reviews in Mineralogy and Geochemistry, 49, 149–220. Mineralogical Society of America and The Geochemical Society, Washington, D.C.

Fenter, P., Geissbühler, P., DiMasi, E., Srajer, G., Sorensen, L.B., and Sturchio, N.C. (2000a) Surface speciation of calcite observed in situ by high-resolution X-ray reflectivity. Geochimica et Cosmochimica Acta, 64, 1221–1228.

Fenter, P., Teng, H., Geissbühler, P., Hanchar, J.M., Nagy, K.L., and Sturchio, N.C. (2000b) Atomic-scale structure of the orthoclase (001)-water interface measured with high-resolution X-ray reflectivity. Geochimica et Cosmochimica Acta, 64, 3663–3673.

Fenter, P., McBride, M.T., Srajer, G., Sturchio, N.C., and Bosbach, D. (2001) Structure of barite (001)- and (210)-water interfaces. Journal of Physical Chemistry B, 105, 8112–8119.

Fenter, P., Cheng, L., Park, C., Zhang, Z., and Sturchio, N.C. (2003) Structure of orthoclase (001)- and (010)-water interfaces by high-resolution X-ray reflectivity. Geochimica et Cosmochimica Acta., 67, 4267–4275.

Franks, F. (2000) Water: A matrix of life, 2nd Edition. Royal Society of Chemistry, Cambridge.

Fuller, C.C., Bargar, J.R., Davis, J.A., and Piana, M.J. (2002) Mechanisms of uranium interactions with hydroxyapatite: Implications for groundwater remediation. Environmental Science and Technology, 36, 158 165.

Gidalevitz, D., Feidenhans'l, R., Smilgies, D.M., and Leiserowitz, L. (1997) X-ray scattering from surfaces of organic crystals. Surface Review and Letters, 4, 721–732.

Gramain, P. and Schaad, P. (2000) Dissolution of Calcium Hydroxyapatite. In N. Kallay, Ed., Interfacial Dynamics, Surfactant Science Series 88, 475–512. Marcel Dekker, New York-Basel.

Hughes, J.M., Cameron, M., and Crowley, K.D. (1989) Structural variations in natural F, OH, and Cl apatites. American Mineralogist, 74, 870–876.

Ishikawa, T. (1997) Surface chemistry of apatites. Hyomen, 35, 388–397.

Ishikawa, T., Wakamura, M., and Kondo, S. (1989) Surface characterization of calcium hydroxyapatite by Fourier transform infrared spectroscopy. Langmuir, 5, 140–144.

Jeanjean, J., Rouchaud, J.C., Tran, L., and Fedoroff, M. (1995) Sorption of uranium and other heavy metals on hydroxyapatite. Journal of Radioanalytical and Nuclear Chemistry Letters, 201, 529–539.

Joris, S.J. and Amberg, C.H. (1971a) The nature of deficiency in nonstoichiometric hydroxyapatites. I. Catalytic activity of calcium and strontium hydroxyapatites. Journal of Physical Chemistry, 75, 3167–3171.

——— (1971b) The nature of deficiency in nonstoichiometric hydroxyapatites. II. Spectroscopic studies of calcium and strontium hydroxyapatites. Journal of Physical Chemistry, 75, 3172–3178.

Liu, Y. and Nancollas, G.H. (1997) Crystallization and colloidal stability of calcium phosphate phases. Journal of Physical Chemistry B, 101, 3464–3468.

Ma, Q.Y., Logan, T.J., and Traina, J. (1995) Lead immobilization from aqueous solutions and contaminated soils using phosphate rocks. Environmental Science Technology, 29, 1118–1126.

McCarthy, M.I., Schenter, G.K., Scamehorn, C.A., and Nicholas, J.B. (1996) Structure and dynamics of the water/MgO interface. Journal of Physical Chemistry, 100, 16989–16995.

Misra, D.N. (1984) Adsorption on and surface chemistry of hydroxyapatite. Plenum Press, New York.

Mkhonto, D. and de Leeuw, N.H. (2002) A computer modelling study of the effect of water on the surface structure and morphology of fluorapatite: introducing a $Ca_{10}(PO_4)_6F_2$ potential model. Journal of Materials Chemistry, 12, 2633–2642.

Modig, K., Pfrommer, B.G., and Halle, B. (2003) Temperature-dependent hydrogen-bond geometry in liquid water. Physical Review Letters, 90, 075502.

Narten, A.H., Danford, M.D., and Levy, H.A. (1967) X-ray diffraction study of liquid water in the temperature range 4–200°C. Faraday Discussions, 43, 97–107.

Ordoñez-Regil, E., Guzmán, E.T.R., and Ordoñez Regil, En. (1999) Surface modification in natural fluorapatite after uranyl solution treatment. Journal of Radioanalytical and Nuclear Chemistry, 240, 541–545.

Park, S.H. and Sposito, G. (2002) Structure of water adsorbed on a mica surface. Physical Review Letters, 89, 85501.

Posner, A.S. (1985) The structure of bone apatite surfaces. Journal of Biomedical Materials Research, 19, 241–250.

Rakovan, J. (2002) Growth and surface structure of apatite. In M. Khon, J. Rakovan, and J. Hughes, Eds., Phosphates: Geochemical, Geobiological and Materials Importance. 48, p. 51–81. Reviews in Mineralogy, Mineralogical Society of America, Washington.

Robinson, I.K. (1986) Crystal truncation rod and surface roughness. Physical Review B, 33, 3830–3836.

Scatena, L.F., Brown, M.G., and Richmond G.L. (2001) Water at hydrophobic surfaces: Weak hydrogen bonding and strong orientation effects. Science, 292, 908–912.

Schlegel, M.L., Nagy, K.L., Fenter, P., and Sturchio, N.C. (2002) Structure of quartz (1010)- and (1011)-water interfaces determined by X-ray reflectivity and atomic force microscopy of natural growth surfaces. Geochimica et Cosmochimica Acta, 66, 3037–3054.

Tanaka, H., Chikazawa, M., Kandori, K., and Ishikawa, T. (2000) Influence of thermal treatment on the structure of calcium hydroxyapatite. Physical Chemistry Chemical Physics, 2, 2647–2650.

Teterin, Yu.A., Teterin, A.Yu., Dementiev, A.P., Lebedev, A.M., Utkin, I.O., Melikhov, I.V., Nefedov, V.I., Berdonosova, D.G., Bek-Uzarov, J., and Vukchevich, L. (2000) X-ray photoelectron study of the interaction of the uranyl group UO_2^{2+} with hydroxylapatite and fluoroapatite in aqueous solutions. Journal of Structural Chemistry, 41, 611 615.

Ward, M.D. (2001) Bulk crystals to surfaces: Combining X-ray diffraction and atomic force microscopy to probe the structure and formation of crystal interfaces. Chemical Reviews, 101, 1697–1725.

Wu, L., Forsling, W., and Schindler, P.W. (1991) Surface complexation of calcium minerals in aqueous solution 1. Surface protonation of fluorapatite-water interfaces. Journal of Colloid and Interface Science, 147, 178–185.

Young, E.J., Myers, A.T., Munson, E.L., and Conklin, N.M. (1969) Mineralogy and geochemistry of fluorapatite from Cerro de Mercado, Durango, Mexico. U.S. Geological Survey Professional Paper, 650-D, D84-D93, U.S. Geological Survey, Washington.

MANUSCRIPT RECEIVED AUGUST 15, 2003
MANUSCRIPT ACCEPTED APRIL 2, 2004
MANUSCRIPT HANDLED BY JILL PASTERIS